4

An Introduction to FY-3/MERSI, Ocean Colour Algorithm, Product and Application

Sun Ling[1], Hu Xiuqing[1], Guo Maohua[2],
Zhu Jianhua[3], Li Sanmei[1] and Ding Lei[4]
[1]*National Satellite Meteorological Centre,*
[2]*National Satellite Ocean Application Service,*
[3]*National Ocean Technology Centre,*
[4]*Shanghai Institute of Technical Physics,*
China

1. Introduction

Ocean colour is the water-leaving radiance in the visible and near-infrared just above the ocean surface owing to selective absorption and scattering by phytoplankton and its pigments such as chlorophyll, as well as dissolved organic matter and suspended particulate matter in the subsurface ocean waters. Ocean colour carries useful information concerning biogeochemical properties of the water body. Ocean colour remote sensing can be applied in investigating the optical properties of upper ocean layers, biological productivity, global carbon and biogeochemical cycles in the oceans.

When an ocean-colour sensor measures the radiance backscattered by the ocean-atmosphere system, the signal it received is largely dominated by the atmosphere. Ocean colour retrieval from satellite measured top-of-the-atmosphere (TOA) radiances over the oceans requires removal of the atmospheric and ocean surface interfering effects, a process termed atmospheric correction which is the key step in ocean colour data processing. Water-leaving radiance is the basic product in ocean colour remote sensing, and can be used to derive the water inherent optical property (IOP) and constituent's concentration, photosynthetically active radiation (PAR), red-tide index. Other oceanic applications such as primary productivity and global carbon can be investigated further. Besides water-leaving radiance, concentration of phytoplankton pigments such as chlorophyll a is another standard ocean colour product. Diffuse attenuation coefficient, fluorescence line height, photosynthetically available radiation, concentrations of particulate organic and inorganic carbon, chromophoric dissolved organic matter and suspended particulate matter can also be provided.

With the advantage of spatial coverage and frequent overpass, satellite instruments are widely used in ocean research at local and regional scales. Since the launch of the Coastal Zone Colour Scanner (CZCS) in 1978, ocean colour remote sensing has been focused on studying the spatial and temporal evolution of phytoplankton in open oceanic areas. The main purpose is to improve our understanding of the carbon cycle and the role of the ocean in climate change. After CZCS, instruments with improved spatial and spectral

characteristics have been deployed on space borne satellites. The Sea-Viewing Wide Field-of-View Sensor (SeaWiFS) provides the oceanographic community an unprecedented opportunity to retrieve ocean colour on a global scale. Then, the Moderate Resolution Imaging Spectrometer (MODIS) with a total of 36 channels continues the ocean colour observation. It is worth mentioning some ocean colour instruments, e.g. Ocean Colour Temperature Scanner (OCTS), Modular Optoelectronic Scanner (MOS), Medium Resolution Imaging Spectrometer (MERIS), Ocean Colour Monitor (OCM) and Global Line Imager (GLI). Geostationary Ocean Colour Imager (GOCI) launched in 2010 allows more frequent data provision.

FengYun-3 (FY-3) is the second generation of Chinese polar-orbit meteorological satellite operating in a near polar, sun-synchronous orbit at an altitude of 836 km. The morning satellite FY-3A (launched on May 27, 2008) with local equator-crossing time of 10:30 A.M. (descending southward) and the afternoon satellite FY-3B (launched on Nov 5, 2010) with local equator-crossing time of 1:30 P.M. (ascending northward) have been in operation. Medium Resolution Spectral Imager (MERSI), a major sensor among its 11 payloads, is a MODIS-like sensor covering visible to infrared spectral region. FY-3/MERSI is capable of making continuous global observations for a broad range of scientific studies of the Earth's system, and ocean colour application is one of its main targets.

In this chapter, an overview of MERSI instrument is presented in section 2. Quantitative remote sensing such as ocean colour is sensitive to sensor's radiometric performance. MERSI can not realize the onboard absolute radiometric calibration in the reflective solar spectral region. Various calibration techniques are adopted to monitor the radiometric degradation and assure calibration accuracy, such as absolute calibration using China Radiometric Calibration Site (CRCS) with in-situ measurements, multi-sites calibration tracking and relative calibration with onboard calibrator. The sensor performance related with ocean colour and primary calibration results in reflective solar spectral bands are briefly introduced in section 3. FY-3A/MERSI ocean colour products consist of water-leaving reflectance retrieved from atmospheric correction algorithm, chlorophyll a concentration, pigment concentration, total suspended mater concentration and absorption coefficient of CDOM and NAP from global and Chinese regional empirical models. The FY-3A/MERSI ocean colour product specification, atmospheric correction algorithm based on lookup tables (LUT) and ocean colour components concentration estimation models are described in section 4. The ocean colour product has been primarily validated against in situ data and the comparison result is given in section 5. Ocean colour product is helpful in understanding the ocean variability and changes with their effects on climatic processes. In section 5, some ocean colour application cases using MERSI data such as algae bloom monitoring and coastal suspended sediment variation are also demonstrated.

2. Overview of MERSI instrument

MERSI is manufactured by Shanghai Institute of Technology and Physics (SITP), Chinese Academy of Sciences (CAS). First serial MERSI (called MERSI-1) onboard the firstly three FY-3 satellites has 20 spectral bands, of which 19 are the reflective solar bands (RSBs) covering the wavelength range of 0.4-2.1 μm and one is the thermal emissive band (TEB) covering 10-12.5 μm. FY-3/MERSI is a cross-track scanning radiometer. There are two calibrator systems inside: a Visible Onboard Calibrator (VOC) for RSBs and a Blackbody (BB) for TEB. Figure 1 shows the instrument photo. MERSI makes earth view observations

via a single-sided 45° scan mirror in concordance with a K mirror (de-rotation) over a scan angle range of ±55° about nadir. It provides a swath of 2900 km cross track by 10 km (at nadir) along track for each scan with multi-detectors (10 or 40), enabling a complete global coverage in one day. MERSI has a nominal ground instantaneous field of view (GIFOV) of 250 m, or 1000 m at nadir. The general information and spectral band specifications are listed in Table 1 and 2. The global moderate-resolution narrow-band observations in 20 spectral bands have provided useful data for scientific studies and applications in land, ocean, and atmosphere.

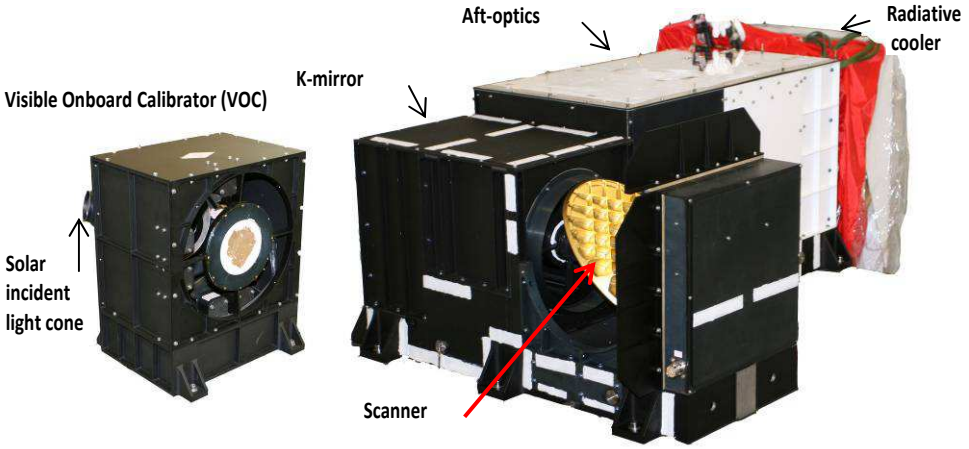

Fig. 1. Instrument photo of MERSI (the left is the VOC and the right is the instrument main component).

Parameters	Specification
Earth scanning	±55.1°±0.1°
Quantization	12 bits
Scanner speed	40 rotations/minute
Scanning stability	<0.5 IFOV (1000m)
Sampling pixels of each scan	2048(1000-m bands); 8192(250-m bands)
Response degradation rate	<20%/3 years
Spectral characterization accuracy	Bias of central wavelength < 10%×band width; out of band response < 3%
Inter-band co-registration	<0.3 pixel
Bright target recovery	≤6 pixels(1000-m bands) ≤24pixels(250-m bands)
MTF	≥0.27(1000-m bands); ≥0.25(250-m bands)
Radiometric calibration accuracy	Visible bands <7%; thermal band<1K(270K)
Detector consistency within one band	Unconsistency≤5-7%

Table 1. General information of MERSI.

Band	Central wavelength(μm)	Band width (μm)	Resolution (m)	NEΔρ(%)/ NEΔT (300K)	Dynamic range (maximum ρ or T)
1	0.470	0.05	250	0.45	100%
2	0.550	0.05	250	0.4	100%
3	0.650	0.05	250	0.4	100%
4	0.865	0.05	250	0.45	100%
5	11.25	2.5	250	0.54K	330K
6	1.640	0.05	1000	0.08	90%
7	2.130	0.05	1000	0.07	90%
8	0.412	0.02	1000	0.1	80%
9	0.443	0.02	1000	0.1	80%
10	0.490	0.02	1000	0.05	80%
11	0.520	0.02	1000	0.05	80%
12	0.565	0.02	1000	0.05	80%
13	0.650	0.02	1000	0.05	80%
14	0.685	0.02	1000	0.05	80%
15	0.765	0.02	1000	0.05	80%
16	0.865	0.02	1000	0.05	80%
17	0.905	0.02	1000	0.10	90%
18	0.940	0.02	1000	0.10	90%
19	0.980	0.02	1000	0.10	90%
20	1.030	0.02	1000	0.10	90%

Table 2. Spectral band specification of MERSI.

Scene radiant flux reflects from the continuously rotating scan mirror at 40 rpm. Energy from the scan mirror strikes the primary mirror (the entrance pupil), goes through a field stop and then onto the secondary mirror. Radiance reflected from the secondary mirror is transmitted to K mirror which is used to remove the rotation of the image due to the rotation by 45° scanner and multi-detector parallel. The K mirror rotates at exactly half the rate of the scanner and uses alternating mirror sides on successive telescope scans. Immediately after K mirror there is a dichroic beam splitter assembly (consisting of three beam splitters) that directs the energy through four refractive objective assemblies and then onto the four focal plane assemblies (FPAs) with their individual band-pass filters. The beam splitters are used to achieve spectral separation, dividing the MERSI spectral domain into four spectral regions: visible (VIS) (412 to 565 nm), near infrared (NIR) (650 to 1030nm), short wavelength infrared (SWIR) (1640 to 2130nm), and long wavelength infrared (LWIR) (12250nm). The SWIR and LWIR FPAs are cooled to approximately 90 K by a passive radiative cooler. All instrument bands, each with multiple detectors (40 and 10 along-track detectors for 250-m and 1000-m band separately) are aligned in the scan direction on focal planes. The VIS and NIR FPAs utilize p-i-n photovoltaic silicon diodes. The SWIR bands have photovoltaic HgCdTe detectors and LWIR band uses photoconductive HgCdTe. The outputs from multiple detectors in each band are added using a time delay and integration (TDI) technique to improve the signal-to-noise ratios (SNRs). The VOC is mounted on the side of the instrument, allowing the scanner to view the VOC's exit when passing over the South Pole. Space view (SV) port is used to provide a zero reference.

3. In-flight performance of solar bands

3.1 Radiometric response change using VOC

MERSI VOC is the first onboard visible calibration experimental device for FengYun series sensors. It is composed of a 6-cm diameter integrating sphere with interior lamp and sunlight import cone, an export beam expanding system with a flat mirror and a parabola to create a collimated beam, and absolute radiance trap detectors (4 detectors with the same filter designs as MERSI bands of 470nm, 550nm, 650nm and 865nm, and one panchromatic detector with no filter). The export parallel light from the expanding system fills the entrance aperture of MERSI and is viewed each scan. Although the VOC can not realize the absolute radiometric onboard calibration, it can be used as a radiometric source to monitor the radiometric response degradation of MERSI.

Figure 2(a) shows the digital number (DN) variation of 5 VOC trap detectors at different time. The degradation of interior lamp illumination appears. Response degradation rates of 19 MERSI solar bands are then derived using the scanning DN and lamp illumination degradation. Figure 2(b) reveals the great degradation of band 1, 8, 9, 10 of MERSI since launch. The greatest degradation is in band 8 (412nm), more than 15% during one year. It has been found that there exist signal anomaly jumps at band 6 and 7. The instrument vendor explained that it was induced by the electronic gain anomaly jump of MERSI SWIR bands. So the degradation status of band 6 and 7 have to be re-evaluated based on the electronic gain levels.

3.2 Vicarious radiometric calibration tracking

China Radiometric Calibration Site (CRCS) for satellite calibration in VIS/NIR bands is located at Dunhuang Gobi desert, centered at 40.65°N, 94.35°E. Annual field campaigns have been routinely carried out at CRCS, and the vicarious calibration (VC) based on synchronous in-situ measurements is the baseline operational calibration approach for Chinese FengYun (FY) series satellites (Hu et al., 2010). Annual CRCS field campaign for MERSI has been conducted since Sep. 2008.

Although the CRCS based vicarious calibration has the accuracy of ~5%, the limited data amount is not enough for frequent and stable in-flight calibration coefficient updates. Multi-sites with stable surface properties have been chosen for radiometric calibration tracking. Gobi and desert targets such as Dunhuang, Libya1(24.42°N, 13.35°E), Libya4(28.55°N, 23.39°E) and Arabia2(20.13°N, 50.96°E) recommended by CEOS/WGCV are used, as well as an ocean site at Lanai(MOBY, 20.49°N,°-157.11E). Surface directional reflectance is calculated using MODIS BRDF products for land sites or taken from MOBY measurements for the ocean site. Aerosol optical depth is taken from MODIS monthly aerosol product. With the V6S model, TOA reflectance (*Ref*) can be calculated. Data within certain days from 5 sites are used to get the calibration coefficient (slope):

$$ARef_i = Ref_i \, (d0/d)^2 \cos(SolZ) = Slope_i \, (DN_i - SV_i), \tag{1}$$

where $ARef_i$ is the TOA apparent reflectance for band i, $SolZ$ is solar zenith angle, $(d0/d)^2$ is earth-sun distance correction factor, $Slope$ is calibration slope, DN and SV are digital numbers of earth observation and space view respectively. Based on the calibration coefficient series, a linear model is used to describe the varying trend of calibration slopes:

$$Slope_i = a_i DSL + b_i, \tag{2}$$

where *DSL* is the day number since launch (May 27, 2008), *a* reflects the degradation rate of response gain (1/*Slope*).

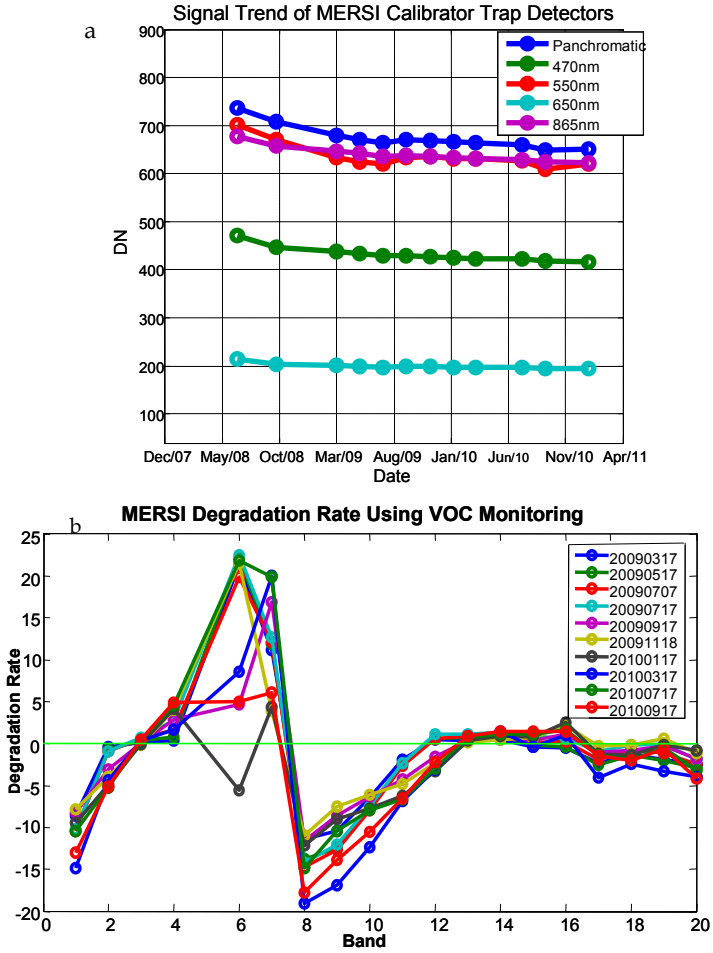

Fig. 2. MERSI VOC's output monitoring by trap detectors (a) and derived response degradation of 19 reflective solar bands (b) from VOC's observation at different dates.

Typical examples of band 1, 2, 3 and 4 are shown in Fig. 3, in which the linear fitting model is shown with black solid line. Band 6 and 7 are omitted because of anomaly electronic gain jumps possibly induced by electrostatic discharge. It can be seen that the calibration coefficients present a linear trend with DSL, and seasonal periodicity exists especially in the short-wave and the water vapor channels. The calibration tracking results are listed in Table 3 using data from Aug. 2008 to Dec. 2010. The short-wave channels have large degradation, especially band 8 with the annual decay rate up to 14%. In the red and near-infrared bands (600 ~ 900nm), e.g. band 3, 4, 13, 14, 15 and 16, the calibration coefficients almost have no

change with the annual decay rate below 1%. The uncertainty (2σ/mean) for the trend analysis is below 5% except for water vapor bands (17, 18 and 19).

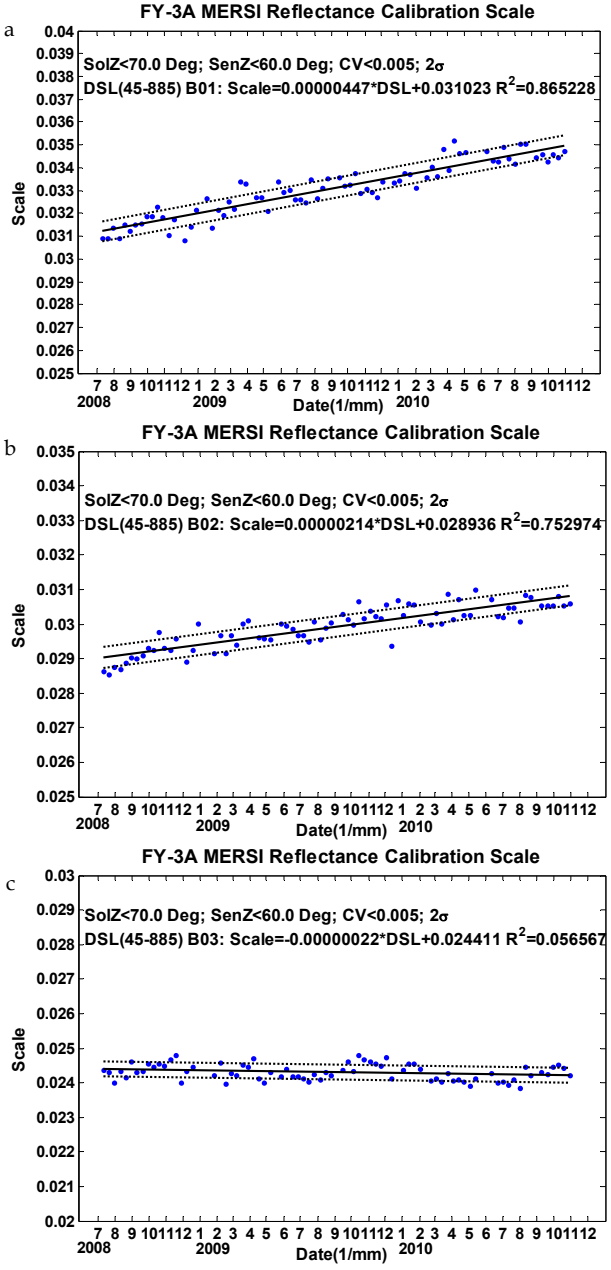

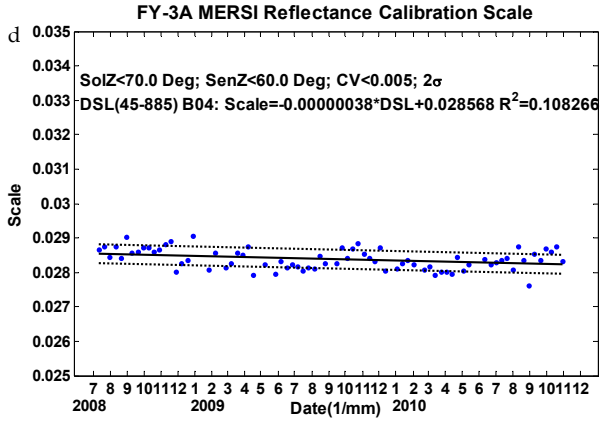

Fig. 3. Calibration coefficient trend of band 1(a), 2(b), 3(c) and 4(d) from multi-sites calibration.

Band	a	b	2σ/mean(%)	Annual Decay Rate(%)
1	4.47E-06	0.0310	2.6694	5.2561
2	2.14E-06	0.0289	2.0388	2.6947
3	-2.19E-07	0.0244	1.8415	-0.3282
4	-3.83E-07	0.0286	1.9638	-0.4895
8	8.61E-06	0.0217	4.3801	14.4623
9	4.78E-06	0.0237	3.4290	7.3481
10	2.87E-06	0.0245	2.4686	4.2702
11	1.91E-06	0.0199	2.2112	3.5070
12	1.16E-06	0.0225	1.7599	1.8896
13	-5.91E-08	0.0223	1.9964	-0.0970
14	-2.39E-08	0.0217	1.8287	-0.0402
15	6.73E-07	0.0276	1.9260	0.8887
16	5.12E-08	0.0211	1.3659	0.0884
17	2.36E-06	0.0243	6.1333	3.5431
18	7.25E-06	0.0262	19.7859	10.0894
19	2.48E-06	0.0233	6.3302	3.8836
20	2.99E-06	0.0253	2.1729	4.3028

Table 3. FY-3A/MERSI solar bands calibration tracking results with multi-sites method.(σ: The standard deviation of difference between calibration coefficients and the linear regression line).

4. Ocean colour product

4.1 Product specification

Several quantitative parameters are provided in FY-3A/MERSI ocean colour product:

- Water-leaving reflectance ($\rho_w = L_u(0^+)/ L_d(0^+)$) for band 8 to 16 retrieved from atmospheric correction algorithm based on LUTs,
- Chlorophyll a (Chla) concentration (CHL1) and pigment concentration (PIG1) from global empirical models,
- Chlorophyll a concentration (CHL2), total suspended mater concentration (TSM), absorption coefficient of CDOM and NAP at 443nm band (YS443) from Chinese regional empirical models.

FY-3A ocean colour product specification is shown in Table 4. The product file format is HDF5. Examples of ocean colour product are shown in Fig. 4.

Type	Projection	Coverage	Spatial Resolution
Day	Geographic Longitude/Latitude	Global, 10°×10° per breadth	0.01°×0.01°
Ten days	Ditto	Global	0.05°×0.05°
Month	Ditto	Global	0.05°×0.05°

Table 4. FY-3A ocean colour product specification.

4.2 Atmospheric correction algorithm

For the ocean-atmosphere system, TOA reflectance measured by the satellite sensor in a spectral band centered at a wavelength λ, $\rho_t(\lambda)$, can be written as a linear sum of various contributions (angular dependencies are omitted):

$$\rho_t(\lambda) = [\rho_w(\lambda)+\rho_{wc}(\lambda)+\rho_g(\lambda)]T_g(\lambda)T_{r+a}(\lambda)+\rho_{atm}(\lambda), \quad (3)$$

$$\rho_{atm}(\lambda) = [\rho_{mix}(\lambda)-\rho_r(\lambda)]T_g(\lambda)+\rho_r(\lambda)T_g'(\lambda), \quad (4)$$

where ρ_w is water-leaving reflectance, ρ_{wc} is whitecap reflectance, ρ_g is sun glint reflectance, T_g is gaseous absorption transmittance, T_g' is gaseous absorption transmittance excluding water vapor, T_{r+a} is scattering transmittance of the Rayleigh and aerosol mixing atmosphere, ρ_{atm} is intrinsic atmospheric reflectance reaching the sensor, ρ_{mix} is reflectance for the Rayleigh and aerosol mixing atmosphere not accounting for absorptive gases, and ρ_r is reflectance for a pure Rayleigh atmosphere not accounting for absorptive gases.

None water-leaving effects are calculated and removed from ρ_t to extract ρ_w. ρ_r is calculated using look-up tables with angles and surface pressure (Sun et al., 2006). T_g together with T_g' is calculated using formulas based on simulations with angles and gases amounts (Sun & Zhang, 2008). ρ_{wc} is estimated using an empirical model with wind speed (Gordon, 1997). ρ_g is estimated using the Cox & Munk model with wind and angles. T_{r+a} is calculated using look-up tables with certain aerosol model, aerosol optical thickness τ_a and angles (Sun, 2005). To determine ρ_{mix}, mainly the aerosol contribution because ρ_r can be calculated in advance, $\tau_a \leftrightarrow \gamma$ ($\gamma=\rho_{mix}/\rho_r$) lookup tables with various aerosol models and angles are used (Sun & Guo, 2006). Seven candidate aerosol models from OPAC database are adopted. The aerosol scattering phase function $P_a(\Theta)$ and normalized aerosol optical thickness $\Delta\tau_a$ are separately shown in Fig. 5.

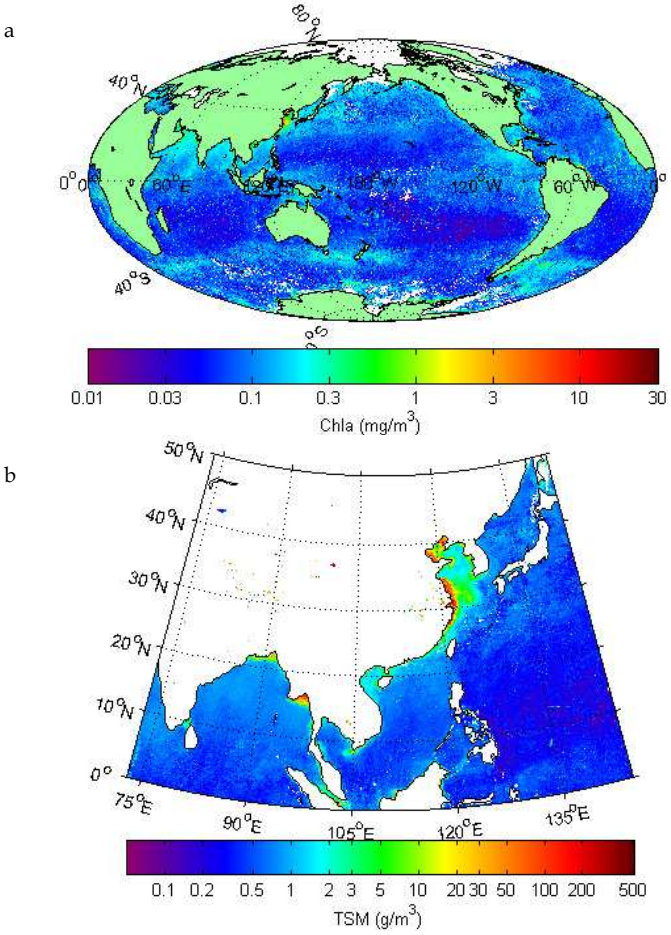

Fig. 4. Monthly mean global Chl-a (a) and TSM (b) around China coast of Feb. 2010.

The water-leaving reflectance at two NIR bands (centered at 765 and 865nm) are assumed zeros. Thus, $\gamma(765)$ and $\gamma(865)$ are obtained from ρ_t. $\tau_a(865)_i$ for 7 aerosol models are calculated using $\tau_a \leftrightarrow \gamma$ lookup tables, and $\tau_a(\lambda)_i$ are extrapolated with the normalized optical thickness $\Delta\tau_a(\lambda)_i$, and $\gamma(765)_i$ are reversely calculated using $\tau_a \leftrightarrow \gamma$ lookup tables. Then, two aerosol models (represented with $i1$ and $i2$) most similar to the actual one are selected according to $\gamma(765)_{i1}<\gamma(765)<\gamma(765)_{i2}$, and the mixing ratio X for interpolation between two aerosols is calculated as $[\gamma(765)-\gamma(765)_{i1}]/[\gamma(765)_{i2}-\gamma(765)_{i1}]$. And then, for the visible and NIR bands, $\gamma(\lambda)_{i1}$ and $\gamma(\lambda)_{i2}$ are calculated from $\tau_a(\lambda)_{i1}$ and $\tau_a(\lambda)_{i2}$, and $\gamma(\lambda)$ is estimated as $(1-X)\gamma(\lambda)_{i1}+X\gamma(\lambda)_{i2}$, and $\rho_{mix}(\lambda)$ can then be calculated. Till now, ρ_w can be calculated from equation (3).

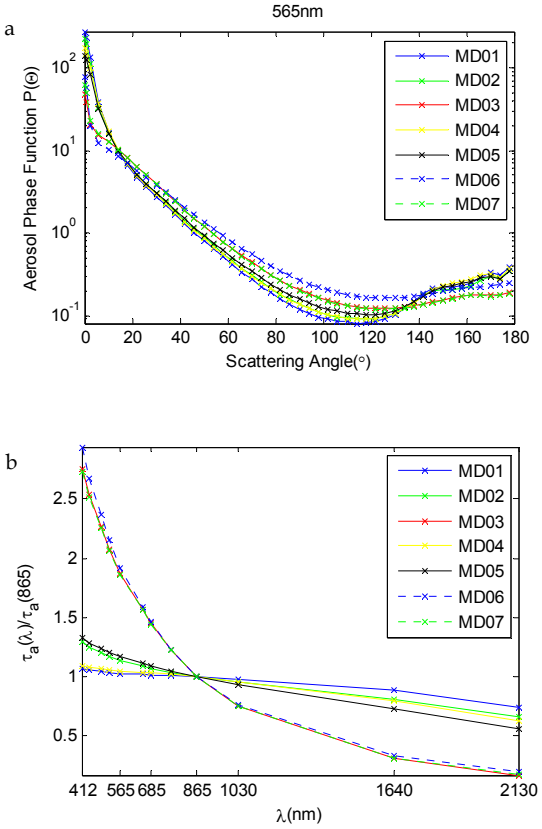

Fig. 5. Aerosol scattering phase function for 565nm band (a) and normalized aerosol optical thickness (b).

4.3 Water constituents concentration estimation models

The MODIS OC3 model is used in global chlorophyll a concentration (CHL1) estimation.

$$\text{Log}(\text{Chl}a) = A_0 + A_1X_c + A_2X_c^2 + A_3X_c^3 + A_4X_c^4, \quad (5)$$

in which,

$$X_c = \text{Log}(\text{MAX}(R_{rs}(443), R_{rs}(488))/R_{rs}(551)),$$

$$A = [0.283, -2.753, 1.457, 0.659, -1.403].$$

The gobal pigment concentration (PIG1) estimation model is derived from the SeaBAM dataset:

$$\text{Log}(\text{PIG}) = A_0 + A_1X_p \quad (N=156, R^2=0.92), \quad (6)$$

in which,

$$X_p = \mathrm{Log}(R_{rs}443/R_{rs}565),$$

$$A = [0.3560, -1.6198].$$

With independent data validation (N=56), the data percentage within relative error of 30% (calculated in log scale) is 71%.

The local models in China coastal region have been constructed with in situ measurements during 2003 spring and fall cruise in the Yellow Sea and the East China Sea organized by the National Satellite Application Service (Tang et al., 2004).

$$\mathrm{Log}(\mathrm{Chl}a) = A_0 + A_1\mathrm{Log}(X_c) + A_2\mathrm{Log}^2(X_c) \quad (R^2=0.87, N=40), \tag{7}$$

in which,

$$X_c = (R_{rs}(443)/R_{rs}(565))(R_{rs}(412)/R_{rs}(490))^b,$$

$$b=-0.75, A=[0.054, -1.46, 0.879].$$

The maximum, minimum and mean Chl*a* are 6.83,0.54 and 1.55 mg/m^3, respectively.

$$\mathrm{Log}(\mathrm{TSM}) = A_0 + A_1\mathrm{Log}(X_s) + A_2\mathrm{Log}^2(X_s) + A_3\mathrm{Log}^3(X_s) \quad (R^2=0.94, N=40), \tag{8}$$

in which,

$$X_s = (R_{rs}(565)+R_{rs}(685))(R_{rs}(490)/R_{rs}(565))^b,$$

$$b=-2, A=[4.309, 4.324, 1.592, 0.212].$$

The maximum, minimum and mean TSM are 340.1, 0.6 and 16.8 g/m^3, respectively.

In China coastal region, the concentration of suspended particle is very high caused by terrestrial inputs, and in-situ data show that the absorption coefficient of none pigment particles is obviously larger than yellow substance.

$$\mathrm{Log}(\mathrm{YS443}) = A_0 + A_1\mathrm{Log}(X_{dg}) + A_2\mathrm{Log}^2(X_{dg}) + A_3\mathrm{Log}^3(X_{dg}) \quad (R^2=0.93, N=40), \tag{9}$$

in which,

$$X_{dg} = (R_{rs}(565)+R_{rs}(685))(R_{rs}(490)/R_{rs}(565))^b,$$

$$b=-2, A=[2.709, 4.286, 1.711, 0.233].$$

The maximum, minimum and mean YS443 are 8.072, 0.052 and 0.583 m^{-1}, respectively.

Independent data are used for validation (N=40). The maximum, minimum and mean for Chl*a*, TSM and YS443 is 3.76, 0.51 and 1.40 mg/m^3; 182.3, 0.5 and 16.6 g/m^3; 6.712, 0.080, and 0.604 m^{-1}, respectively.

The mean relative error

$$1/N\sum_{i=1}^{N}|(X_i^{Mod}-X_i^{Mea})/X_i^{Mea}|$$

is 19.3%, 19.3%, and 26.1%, and the data percentage within relative error of 30% is 67%, 80% and 57% for Chl*a*, TSM and YS443 respectively.

5. Product validation and application

5.1 Primary validation

By comparing with in situ data collected in Feb. 2009, the FY-3A/MERSI ocean colour product was preliminarily validated. But only two match-ups were available, whose time differences were less than 5 minutes. The RMS difference and percentage difference values were given in Table 5. The ρ_w at 443, 520 and 565 nm was systematically overestimated, while ρ_w at 490 nm was underestimated.

	ρ_w					Chl*a*	TSM
	412	443	490	520	565		
RMSD	0.005	0.004	0.004	0.003	0.003	0.023	0.095
RMSPD(%)	21.3	18.9	20.9	30.2	48.2	9.4	10.1

Table 5. FY-3A ocean colour product primary validation result.

5.2 Algae bloom monitoring

FY-3A/MERSI is a nice sensor for algae bloom monitoring. In the late spring and early summer 2008, a severe *enteromorpha prolifera* bloom erupted in the Yellow Sea and the sea area of Qingdao Olympic regatta was severely interfered. A massive algae clearing action was organized in which FY-3A/MERSI played an important role in determining algae distribution, moving route, and directing in situ salvage. Figure 6 showed one false colour MERSI image (RGB with band 3/4/1) on June 28, 2008 (Sun et al., 2010).

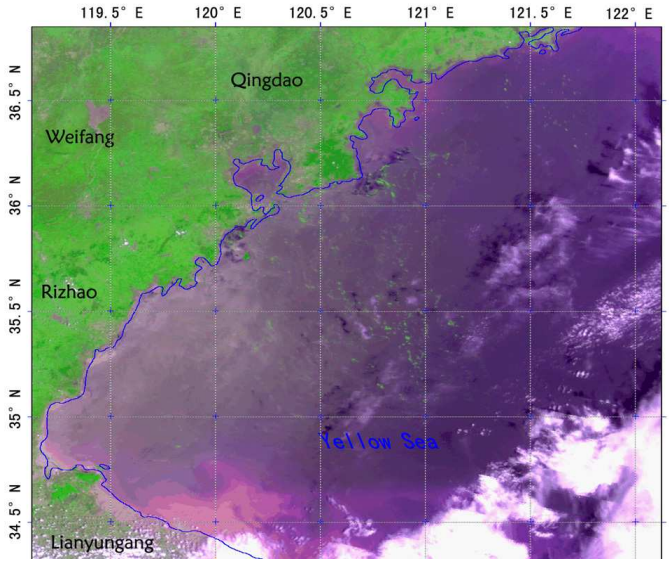

Fig. 6. Algae bloom captured on June 28, 2008 around Qingdao.

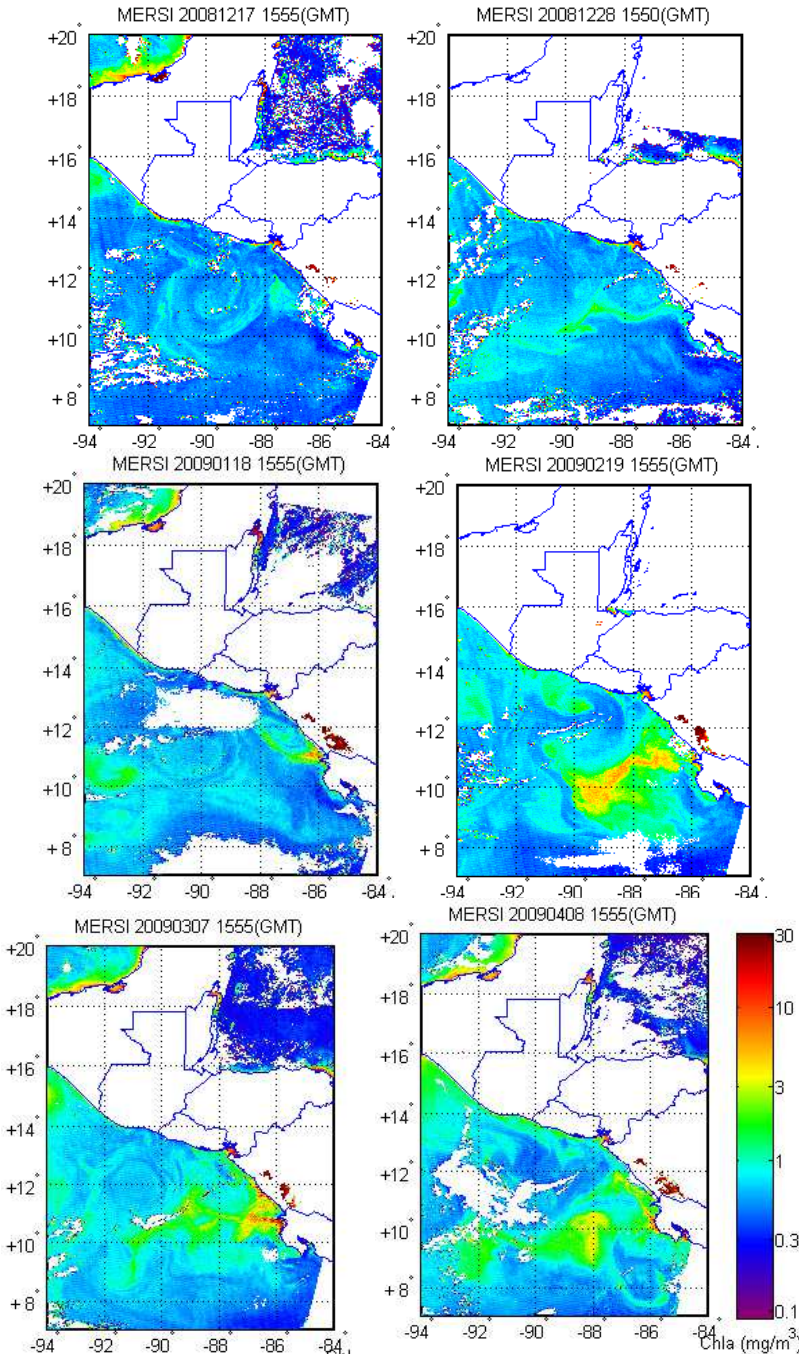

Fig. 7. Red tide process in Central America.

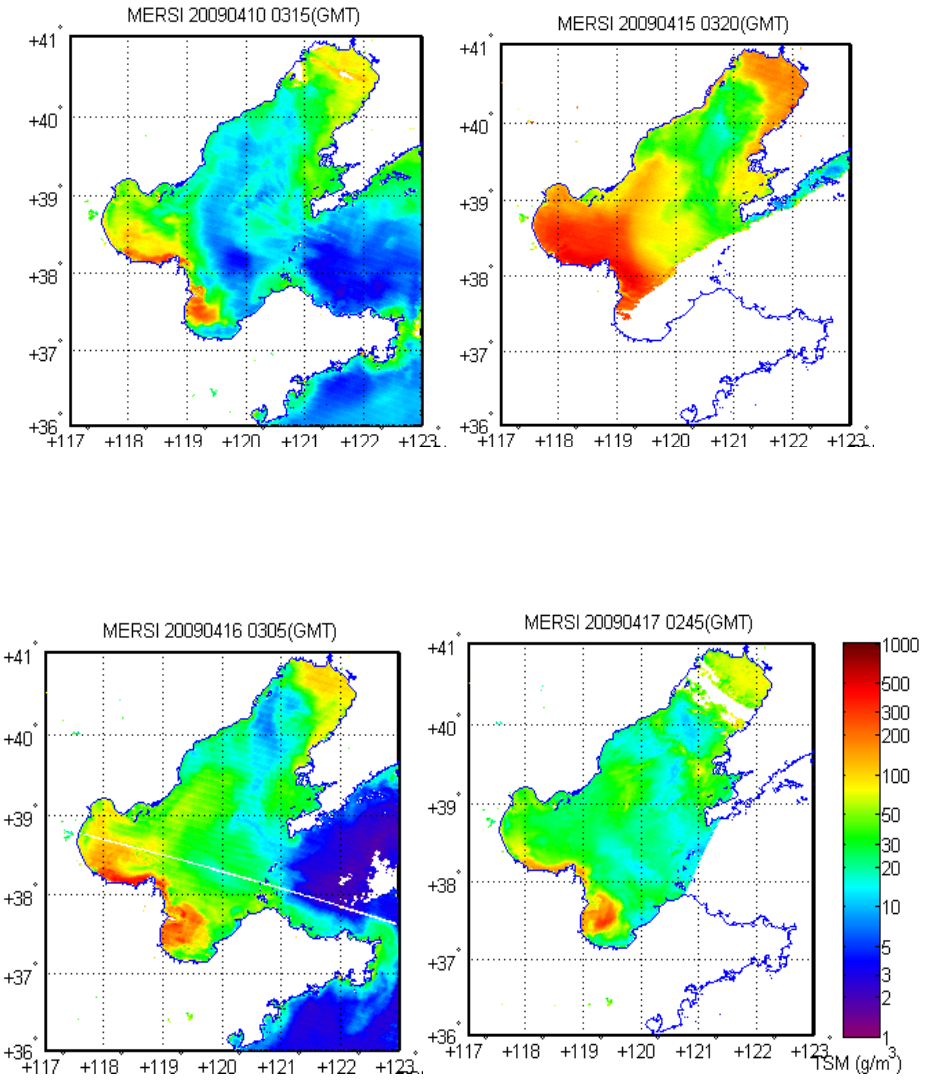

Fig. 8. Suspended particle concentration variation caused by a storm surge at Bohai Sea.

From the end of 2008, a serious HAB attack the Pacific coastal region of the Central America, especially around Costa Rica, Guatemala, El Salvador and Nicaragua. Figure 7 showed this red tide developing process using FY-3A Chl*a* product.

5.3 Suspended sediment variation

In the early morning of Apr.15, 2009, a large storm surge suddenly happened in Bohai Sea, the eleven to twelve level wind rapidly resuspended the marine sediment and changed the suspended particle concentration distribution in the Bohai Sea, especially Bohai Bay and Laizhou Bay. Figure 8 showed this process using the FY-3A TSM product.

6. Conclusion

FY-3A/MERSI is the milestone sensor for Chinese meteorological satellite beyond it's previous instruments. It adopted a special 45° mirror scanning and de-rotation techniques with K mirror which can do multiple detectors scanning. One of the instrument's most outstanding features is that it can provide no gap global observation with its large coverage swath as well as five 250-m bands. The MERSI's global mission will make a major contribution to scientific projects that seek to understand the role of the land, atmosphere and ocean in the climate system and will further increase our ability to forecast change through modeling.

FY-3A/MERSI is the first Chinese sensor having the ability to make ocean colour global coverage. Ocean colour remote sensing is sensitive to sensor's radiometric performance. The MERSI VOC is the first experimental onboard calibrator for visible bands and provides a good way to monitor the relative radiometric response change at visible bands. The based-line calibration approach is VC based on synchronous in-situ measurements, and has been conducted annually using Dunhuang CRCS site in summer since 2008. Although the CRCS based vicarious calibration has the accuracy of ~5%, the limited data amount is not enough for frequent and stable in-flight calibration coefficient updates. Multi-sites with stable surface properties have been chosen for radiometric calibration tracking. It reveals that the short-wave bands have large degradation, especially band 8 with the annual decay rate up to 14%. In the red and near-infrared bands (600 ~ 900nm), e.g. band 3, 4, 13, 14, 15 and 16, the calibration coefficients almost have no change with the annual decay rate below 1%.

FY-3A/MERSI ocean colour products consist of water-leaving reflectance, chlorophyll a concentration (CHL), total suspended mater concentration (TSM) and absorption coefficient of CDOM and NAP (YS443) derived from atmospheric correction algorithm based on lookup tables (LUT) and global and Chinese regional empirical models for ocean colour components concentration estimation. By comparing with in situ data, the FY-3A/MERSI ocean colour product has been preliminarily validated. The ρ_w at 443, 520 and 565 nm was systematically overestimated, while ρ_w at 490 nm was underestimated. The RMS percentage difference for Chl*a* and TSM are 9.4% and 10.1%, respectively.

Ocean colour product is helpful in understanding the ocean variability and changes with their effects on climatic processes. MERSI data have shown good application ability at

ocean colour aspect, such as monitoring of algae bloom and coastal suspended sediment variation.

Although various calibration methods have been used to assure data accuracy, there is still much work to be done to acquire high quality radiometric data. And more validation work is needed to be carried out in the near future. The FY-3A/MERSI data (from L1B to L3) is public, and can be searched and ordered from the website (http://fy3.satellite.cma.gov.cn).

7. Acknowledgment

The authors would like to thank Song Qingjun and all participants in the 2009 Nanhai Cal/Val Campaign conducted by National Satellite Ocean Service for the in-situ dataset. This research is supported by National Key Basic Research Science Foundation ("973" project) of China under contracts No. 2010CB950803 and 2010CB950802, the National Natural Science Foundation of China under contract No. 40606043 and Meteorological Special Project under contract No. GYHY200906036.

8. References

Gordon, H. R. (1997). Atmospheric correction of ocean colour imagery in the earth observing system era. *J. Geophys. Res.*, Vol.102, No.D14, pp. 17081-17106, ISSN 0148–0227

Hu, X., Liu, J., Sun, L., Rong, Z., Li, Y., Zhang, Y. , et al. (2010). Characterization of CRCS Dunhuang Test Site and Vicarious Calibration Utilization for Fengyun (FY) Series Sensors, *Can. J. Remote Sensing*, Vol. 36, No. 5, (October 2010), pp. 566–582, E-ISSN 1712-7971

Sun, L. & Guo, M. (2006). Atmospheric correction for HY-1A CCD in Case 1 waters. *Proceedings of SPIE, Remote Sensing of the Environment: 15th National Symposium on Remote Sensing of China,* Vol. 6200, pp. 20-31, ISBN 0-8194-6256-X, Guiyang, China, August 19-23, 2005

Sun, L. & Zhang, J. (2008). Influence analysis of gaseous absorption on "HY-1A" CZI data processing: Simulation and correction for Rayleigh scattering. *ACTA Oceanologica Sinica*, Vol.27, No.6, (December 2008), pp. 102-114, ISSN 0253-505X

Sun, L. (2005). Atmospheric correction and water constituent retrieval for HY-1A CCD. PhD dissertation (in Chinese). Qingdao: Institute of Oceanology, Chinese Academy of Science, 67-69

Sun, L., Guo, M., Li, S., & Zhao, W. (2010). Enteromorpha Prolifera monitoring with FY-3A MERSI around the sea area of Qingdao. *Remote Sensing Information*, No.1, (February 2010), pp.64-68, ISSN 1000-3177

Sun, L., Zhang, J. & Guo, M. (2006). Rayleigh lookup tables for HY-1A CCD data processing. *J. Remote Sens.*, Vol.10, No.3, (June 2006),pp. 306-311, ISSN 1007-4619

Tang, J., Wang, X., Song, Q., Li, T., Chen, J., Huang, H. & Ren, J. (2004). The statistic inversion algorithms of water constituents for the Huanghai Sea and the East China Sea. *ACTA Oceanologica Sinica*, Vol.23, No.4, (August 2004), pp. 617-626, ISSN 0253-505X

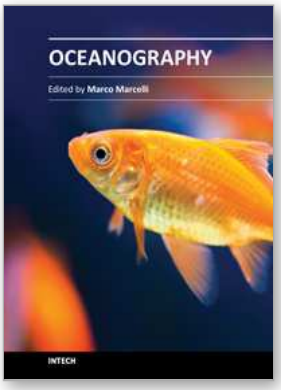

Oceanography

Edited by Prof. Marco Marcelli

ISBN 978-953-51-0301-1
Hard cover, 348 pages
Publisher InTech
Published online 23, March, 2012
Published in print edition March, 2012

How inappropriate to call this planet Earth when it is quite clearly Ocean (Arthur C. Clarke). Life has been originated in the oceans, human health and activities depend from the oceans and the world life is modulated by marine and oceanic processes. From the micro-scale, like coastal processes, to macro-scale, the oceans, the seas and the marine life, play the main role to maintain the earth equilibrium, both from a physical and a chemical point of view. Since ancient times, the world's oceans discovery has brought to humanity development and wealth of knowledge, the metaphors of Ulysses and Jason, represent the cultural growth gained through the explorations and discoveries. The modern oceanographic research represents one of the last frontier of the knowledge of our planet, it depends on the oceans exploration and so it is strictly connected to the development of new technologies. Furthermore, other scientific and social disciplines can provide many fundamental inputs to complete the description of the entire ocean ecosystem. Such multidisciplinary approach will lead us to understand the better way to preserve our "Blue Planet": the Earth.

How to reference

In order to correctly reference this scholarly work, feel free to copy and paste the following:

Sun Ling, Hu Xiuqing, Guo Maohua, Zhu Jianhua, Li Sanmei and Ding Lei (2012). An Introduction to FY-3/MERSI, Ocean Colour Algorithm, Product and Application, Oceanography, Prof. Marco Marcelli (Ed.), ISBN: 978-953-51-0301-1, InTech, Available from: http://www.intechopen.com/books/oceanography/an-introduction-to-fy-3-mersi-ocean-colour-algorithm-product-and-application

INTECH
open science | open minds

InTech Europe
University Campus STeP Ri
Slavka Krautzeka 83/A
51000 Rijeka, Croatia
Phone: +385 (51) 770 447
Fax: +385 (51) 686 166
www.intechopen.com

InTech China
Unit 405, Office Block, Hotel Equatorial Shanghai
No.65, Yan An Road (West), Shanghai, 200040, China
中国上海市延安西路65号上海国际贵都大饭店办公楼405单元
Phone: +86-21-62489820
Fax: +86-21-62489821